CD4$^+$ T-cell Immunity in the Peripheral Blood Correlates with Response to Anti-PD-1 Therapy

Hiroshi Kagamu[1], Shigehisa Kitano[1,2], Ou Yamaguchi[1], Kenichi Yoshimura[3], Katsuhisa Horimoto[4], Masashi Kitazawa[4], Kazuhiko Fukui[4], Ayako Shiono[1], Atsuhito Mouri[1], Fuyumi Nishihara[1], Yu Miura[1], Kosuke Hashimoto[1], Yoshitake Murayama[1], Kyoichi Kaira[1], and Kunihiko Kobayashi[1]

ABSTRACT

Accumulating evidence indicates that CD8$^+$ T cells in the tumor microenvironment and systemic CD4$^+$ T-cell immunity play an important role in mediating durable antitumor responses. We longitudinally examined T-cell immunity in the peripheral blood of patients with non–small lung cancer and found that responders had significantly ($P < 0.0001$) higher percentages of effector, CD62L^{low} CD4$^+$ T cells prior to PD-1 blockade. Conversely, the percentage of CD25$^+$FOXP3$^+$ CD4$^+$ T cells was significantly ($P = 0.034$) higher in nonresponders. We developed a formula, which demonstrated 85.7% sensitivity and 100% specificity, based on the percentages of CD62L^{low} CD4$^+$ T cells and CD25$^+$FOXP3$^+$ cells to predict nonresponders. Mass cytometry analysis revealed that the CD62L^{low} CD4$^+$ T-cell subset expressed T-bet$^+$, CD27$^-$, FOXP3$^-$, and CXCR3$^+$, indicative of a Th1 subpopulation. CD62L^{low} CD4$^+$ T cells significantly correlated with effector CD8$^+$ T cells ($P = 0.0091$) and with PD-1 expression on effector CD8$^+$ T cells ($P = 0.0015$). Gene expression analysis revealed that *CCL19, CLEC-2A, IFNA, IL7, TGFBR3, CXCR3*, and *HDAC9* were preferentially expressed in CD62L^{low} CD4$^+$ T cells derived from responders. Notably, long-term responders, who had >500-day progression-free survival, showed significantly higher numbers of CD62L^{low} CD4$^+$ T cells prior to PD-1 blockade therapy. Decreased CD62L^{low} CD4$^+$ T-cell percentages after therapy resulted in acquired resistance, with long-term survivors maintaining high CD62L^{low} CD4$^+$ T-cell percentages. These results pave the way for new treatment strategies for patients by monitoring CD4$^+$ T-cell immune statuses in their peripheral blood.

Introduction

Programmed cell death 1 (PD-1)/PD-ligand 1 (PD-L1) blockade using mAb has led to markedly prolonged overall survival (OS) of patients with metastatic cancers, including melanoma, head and neck cancer, renal cell carcinoma, gastric cancer, and non–small cell lung cancer (NSCLC; refs. 1–7). Five-year follow-up data reveal that 16% of patients with advanced NSCLC treated with anti-PD-1, nivolumab, survive for >5 years even after discontinuing nivolumab treatment; however, clinical trial results consistently indicate that approximately 40% of patients with NSCLC exhibit early disease progression in the 3 months post PD-1 blockade with no clinical benefit (6–9). Thus, patients with NSCLC fall into three distinct subgroups: nonresponders showing early disease progression, long-term survivors achieving durable disease control, and short-term responders. We hypothesized that these subgroups respond differently to PD-1 blockade therapy owing to patient population specific immunologic patterns.

Tumor-infiltrating lymphocyte analysis of patients reveals that PD-1$^+$ CD8$^+$ T cells play a critical role in antitumor immune responses and that they could be a biomarker to predict antitumor responses of immune checkpoint inhibitors (10–12). However, systemic immune responses comprising of CD62L^{low}CD44$^+$CD69$^+$CD90$^+$CD27^{low}T-bet$^+$CD4$^+$ T cells are required to establish antitumor immunity and subsequently eradicate tumors in murine models (13). These two concepts are not contradictory, as CD4$^+$ T cells, especially Th1 cells, can enhance the functions of cytotoxic CD8$^+$ T cells (CTL), including clonal expansion, memory differentiation, migratory and invasive potential, and CTL activity, differentiation, and survival (14). The cancer immunity cycle suggests that durable antitumor immunity requires continuous T-cell priming by cancer antigens released by dying cancer cells and that primed CTL must migrate through peripheral blood to invade into cancer tissues and kill tumor cells (10). Thus, CD4$^+$ T-cell help could enhance the cancer immunity cycle. CD4$^+$ T cells play an important role in antitumor immunity of murine models, and CD4$^+$ T cells that recognize cancer neoepitopes have been identified in melanoma (5, 8, 11, 12). CD4$^+$ T cells in the peripheral blood correlate with clinical response to PD-1 blockade in patients with melanoma (13). However, it is still unclear whether systemic CD4$^+$ T-cell immunity plays a role in human antitumor immune responses, including patients with lung cancer treated with anti-PD-1.

Antitumor effector T cells are primed at secondary lymphoid organs and migrate through bloodstream to get to target cells (15). A defining feature of antigen-primed T cells, including effector and effector memory T cells, is the downregulated expression of homing receptors, such as CD62L and C-C chemokine receptor 7 (CCR7), that allows cells to migrate to secondary lymphoid tissues (16). Thus, the CD62L^{low} phenotype has been used to identify primed T cells (17). A small CD62L^{low} T-cell subpopulation in tumor-draining lymph nodes exclusively contain all the antitumor T cells and CD62L^{low} CD4$^+$ T cells isolated from tumor-draining lymph nodes mediate potent antitumor reactivity when intravenously transferred (18, 19). The ratio of CD62L^{low} CD4$^+$ T cells to regulatory CD4$^+$ T cells (Treg) that constitutively express IL2 receptor α chain (CD25) and transcription factor forkhead box p3 (FOXP3) in peripheral blood

[1]Division of Respiratory Medicine, Saitama Medical University International Medical Center, Hidaka, Saitama, Japan. [2]Department of Experimental Therapeutics, National Cancer Center Hospital, Tokyo, Japan. [3]Innovative Clinical Research Center, Kanazawa University, Kanazawa, Japan. [4]Molecular Profiling Research Center for Drug Discovery, National Institute of Advanced Industrial Science and Technology, Koto-ku, Tokyo, Japan.

Note: Supplementary data for this article are available at Cancer Immunology Research Online (http://cancerimmunolres.aacrjournals.org/).

Corresponding Author: Hiroshi Kagamu, Saitama Medical University International Medical Center, 1397-1 Yamane, Hidaka, Saitama 350-1298, Japan. Phone/Fax: 81-42-984-4581; E-mail: kagamu19@saitama-med.ac.jp

Cancer Immunol Res 2020;8:334–44

doi: 10.1158/2326-6066.CIR-19-0574

mononuclear cells (PBMC) correlated with disease stage and prognosis in patients with SCLC (20). Treg-mediated attenuation of antitumor immunity resulted in hyperprogressive disease upon PD-1 blockade (21).

In this study, we analyzed PBMCs to explore the T-cell immunity of 171 patients with NSCLC who were scheduled for nivolumab treatment, developing a prediction formula based on the CD62L^{low} CD4$^+$ T-cell and Treg percentages that distinguished nonresponders presenting early disease progression. A discovery cohort of 40 patients and a validation cohort of 86 patients confirmed the high sensitivity and specificity of the formula. We found that CD62L^{low} CD4$^+$ T cells belonged to the T-bet$^+$ CD27$^-$CXCR3$^+$ Th1 subpopulation and correlated with PD-1$^+$ CD8$^+$ T cells. Finally, the percentages of CD62L^{low}CD4$^+$ T cells correlated with long-term survival in patients with NSCLC.

Materials and Methods

Patients

This study included 171 consecutive patients with NSCLC from a single institution, Saitama Medical University International Medical Center (Saitama, Japan) from February 2016 to August 2018. After enrollment, 28 patients were excluded because no evaluable PBMC samples were available for them. Seventeen patients were excluded because the antitumor effect could not be assessed at 9 weeks after nivolumab therapy (**Fig. 1A**). The patient data were divided into two parts to obtain a discovery cohort of 40 patients and an independent validation cohort of 86 patients (**Table 1**). The patients received nivolumab at a dose of 3 mg/kg body weight every two weeks. Tumor response was assessed by using Response Evaluation Criteria in Solid Tumors (RECIST), version 1.1, at week 9 and every 8 weeks thereafter. The cutoff for data collection was May 17, 2019. All specimens were collected after obtaining written informed consent approved by the Internal Review Board of Saitama Medical University International Medical Center in accordance with the Declaration of Helsinki.

Blood sample analysis

Samples were collected into heparinized CPT Vacutainer tubes (Becton Dickinson Vacutainer Systems) and spun at 1,500 × *g* for 20 minutes at room temperature to separate PBMCs from erythrocytes and granulocytes over a Ficoll gradient. PBMCs were frozen at −80°C in Cellbanker2 (Nippon Zenyaku Kogyo Co., Ltd.) and the frozen cells were transferred into a liquid nitrogen tank within a week. For T-cell subset analyses, cells were incubated for 32–48 hours in culture medium consisting of RPMI1640 and 10% FCS before cell staining.

Cells were stained with these mAbs using the FACS Calibur: fluorescein isothiocyanate (FITC)-conjugated anti-CD3 (HIT3a) and anti-CD4 (RPA-T4), phycoerythrin (PE)-conjugated anti-CD8 (RPA-T8) and anti-CD25 (M-A251), PE-Cy7-conjugated anti-CD25 (M-A251), PE-Cy5-conjugated anti-CD62L (Dreg 56; all from BD Pharmingen), and FITC-conjugated anti-CD62L (Dreg 56; eBioscience). The mAbs used for LSR Fortessa analysis are listed in Supplementary Table S1A and S1B. Cell-surface phenotypes were analyzed by direct immunofluorescence staining of 1×10^6 cells with fluorophore-conjugated mAbs. In brief, cells were stained with fluorophore-conjugated mAbs in 100 μL of FACS buffer, PBS supplemented with 5% FCS, for 30 minutes at 4°C. Samples were immediately washed twice with 1.0 mL FACS buffer. Samples were prepared for intracellular staining using a FoxP3 fix and permeabilization kit according to the manufacturer's instruction (eBioscience) and stained at 4°C. After washing twice with FACS Buffer, samples were fixed using 0.5% paraformaldehyde in PBS. The gating strategy is shown in Supplementary Fig. S1. From each sample, 10,000 cells were analyzed using a FACS Calibur and LSR Fortessa flow microfluorometer (Becton Dickinson) and FlowJo software.

Cell purification

PBMCs were obtained from two patients from each responder group: partial response (PR), stable disease (SD), and progressive disease (PD). CD4$^+$ T cells were purified through negative selection by using human CD4$^+$ T-cell isolation kits (Dynabeads Untouched Human CD4 T Cells Kit, 11346D) according to the manufacturer's instruction (Dynal Biotech). CD4$^+$ T cells were further separated into CD62L^{high} and CD62L^{low} cells by using anti-CD62L mAb-coated microbeads and a MACS system (Miltenyi Biotec), following the manufacturer's suggested procedure. Cell purities were all >90% with FCM analysis.

Microarray analysis

CD62L^{high} CD4$^+$ and CD62L^{low} CD4$^+$ T cells in PBMCs purified as described in cell purification method from the two of PR, SD, and PD patients. Total RNA was isolated from purified T cells, using TRIzol reagent (Thermo Fisher Scientific) according to the manufacturer's instruction. Subsequently, cDNA and cRNA were synthesized and single-stranded cDNA (ssDNA) was labeled, according to the manufacturer's instructions, using a WT Plus Reagent Kit (902280, Thermo Fisher Scientific). Total RNA (0.5 μg) was reverse-transcribed into cDNA and then synthesized into cRNA, and ssDNA was reverse-transcribed from 15 μg of cRNA and then labeled; 1.8 μg of labeled ssDNA was hybridized with microarrays according to the manufacturer's instruction (Clariom S Assay, human kit, 602969; Thermo Fisher Scientific) in a GeneChip Hybridization Oven 645. Hybridized arrays were scanned using a GCS3000 7G System (Thermo Fisher Scientific). The accession number ID of the gene-expression data is GSE103157.

To identify the gene signatures from the two sets of gene expression data, we estimated the difference of gene expression between the two sets as follows. First, we performed the outlier test (22) for all values of probes, and then calculated a z-score for each probe by using the average and the variance of the probe values except for outliers, because the influence of outliers is more important if the statistic examined is less robust (23). To compare the z-scores of the two gene sets, the z-score of each gene was transformed into probability, and then each difference of gene probability between the two sets, p^d, was calculated thus:

$$p_k^d = \left| p\left(z_k^a\right) - p\left(z_k^b\right) \right| = \left| \frac{1}{\sqrt{2\pi}} \int_{-\infty}^{z_k^a} e^{-\frac{z}{2}} dz - \frac{1}{\sqrt{2\pi}} \int_{-\infty}^{z_k^b} e^{-\frac{z}{2}} dz \right|$$

where the k-th gene between the two gene sets, a and b, was compared. Using the above formula, we can estimate the difference of one gene in two gene sets, *a* and *b*, regardless of the differing dynamic ranges of the two gene sets in respective measurement conditions. In general, the threshold of gene probability difference, p_k^d, to select the signature depends on the study, and in this analysis, we selected the genes featuring $p_k^d > 0.2$ as the gene signature (23).

Mass cytometry

The mAbs used for Helios mass cytometer analysis are listed in Supplementary Table S1B. Up to 2.5×10^6 cells were stained with mass cytometry antibodies according to the manufacturer's instructions (Fluidigm Corp.). In brief, a 50 μL volume of 198Pt monoisotopic

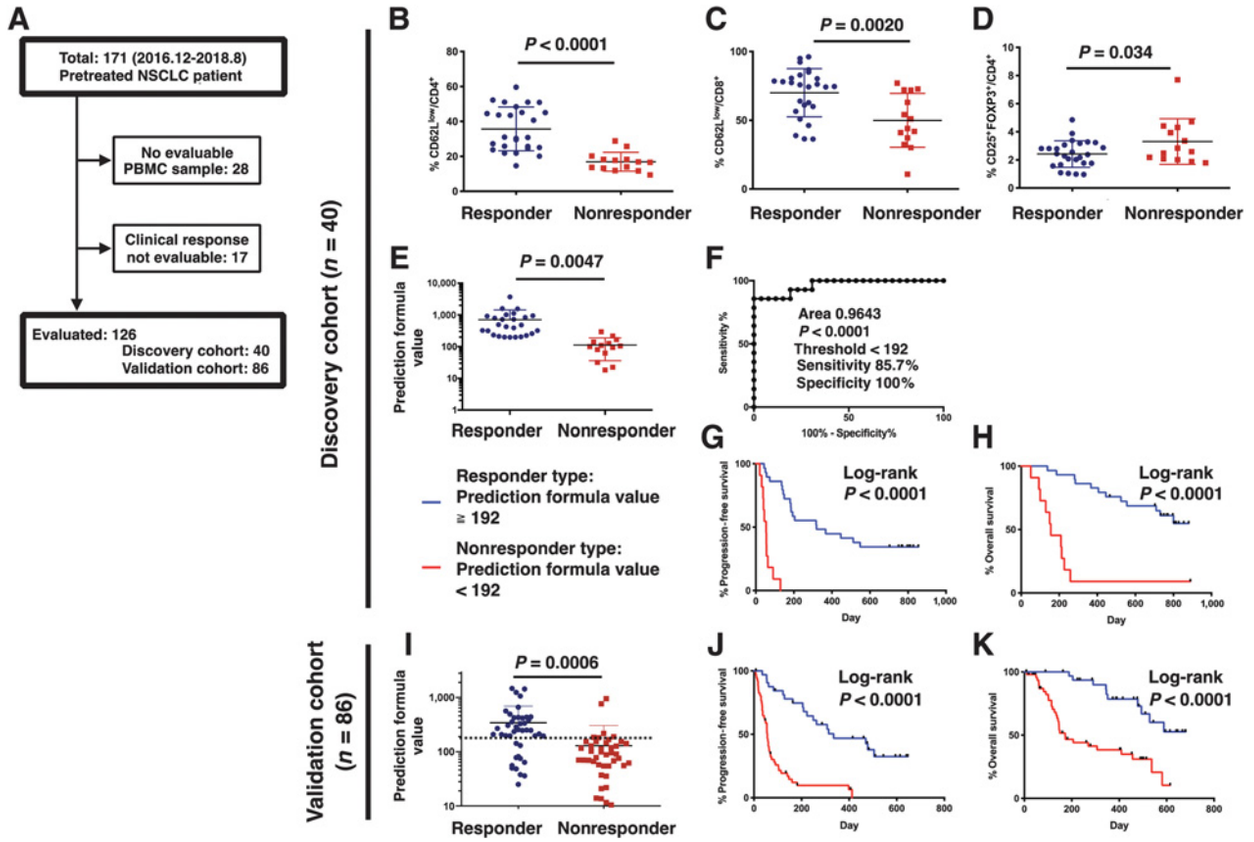

Figure 1.

Correlation of T-cell subpopulations with NSCLC patient response to nivolumab therapy. **A,** CONSORT diagram describing patients and patient samples obtained. **B–D,** Differences in PBMC subpopulations in responders who achieved PR or SD ($n = 26$) and nonresponders ($n = 14$) presenting disease progression by 9 weeks after nivolumab therapy. **B** and **C,** Percentages of $CD62L^{low}$ cells in total populations of $CD4^+$ and $CD8^+$ cells, respectively. **D,** Percentage of $CD25^+FOXP3^+$ cells in total population of $CD4^+$ cells. **E,** Prediction formula values for discovery cohort patients. The formula, X^2/Y, was based on the percentages of $CD62L^{low}$ cells (X) and $CD25^+FOXP3^+$ cells (Y) in the total population of $CD4^+$ cells. **F,** Receiver operating characteristic curve of the formula that predicted nonresponders in the discovery cohort ($n = 40$). Sensitivity and specificity at the threshold value of the formula (192) were 85.7% and 100% ($P < 0.0001$), respectively. **G,** Progression-free survival curves of discovery cohort patients diagnosed as nonresponders or responders based on the threshold value of the prediction formula (192). **H,** OS curves of the discovery cohort. **I,** Prediction formula values for validation cohort patients. **J,** Progression-free survival curves of validation cohort patients. **K,** OS curves of validation cohort patients. In **B–E** and **I**, data were presented as means ± SEM, and symbols indicate values for individual patients. Statistical significance of differences was assessed using Student two-tailed *t* test (**B–E**, **I**) or log-rank test (**G**, **H**, **J**, **K**).

cisplatin (Fluidigm) in PBS was added directly for a final concentration of 2.5 μmol/L for 5 minutes. Samples were immediately washed twice with Maxpar Cell Staining Buffer (Fluidigm). Cells were stained with mass cytometry antibodies for 30 minutes at room temperature. For intracellular staining, samples were prepared using a FoxP3 fix and permeabilization kit as described above before staining. After washing twice with Maxpar Cell Staining Buffer, samples were fixed using 1.6% paraformaldehyde in PBS supplemented with 100 nmol/L iridium nucleic acid intercalator (Fluidigm Corp.). Following fixation, cells were washed twice with 0.5% BSA PBS and 0.1% BSA water and resuspended in 0.1% BSA water. Twenty-thousand cells were analyzed using a Helios and Cytobank software to obtain viSNE analysis and heatmap analysis.

Statistical analysis

SAS 9.4 (SAS Institute Inc.) and Prism 8 (GraphPad) were used to conduct statistical analyses. Data are expressed as means ± SEM, unless otherwise indicated. Tests for differences between two populations were performed using a Student *t* test. Multiple-group comparison was performed using one-way ANOVA with Tukey *post hoc* analysis. The prediction formula was developed by using the discovery cohort data with a logistic regression model. The performance of the prediction formula was evaluated using the independent validation-cohort data. Survival curves were estimated using the Kaplan–Meier method. All *P* values were two-sided, and $P < 0.05$ was considered statistically significant.

Results

Differences in $CD62L^{low}$ T-cell subset percentages between responders and nonresponders

This study included 171 consecutive patients with NSCLC who were treated with nivolumab at a single institution, Saitama Medical University International Medical Center (Saitama, Japan), from February 2016 to August 2018 (**Fig. 1A**). Because this is an observational study on practical treatment, all the patients were pretreated with

Table 1. Baseline characteristics and objective response.

Patient characteristics	Discovery cohort $n = 40$	Validation cohort $n = 86$
Age, years		
Median	67	69
Range	51–84	31–85
Sex, *n* (%)		
Male	26 (65.0)	67 (77.9)
Female	14 (35.0)	19 (22.1)
Histology, *n* (%)		
Squamous	10 (25.0)	24 (27.9)
Nonsquamous	30 (75.0)	62 (72.1)
Smoking history, *n* (%)		
Current or former smoker	29 (72.5)	68 (79.1)
Never smoked	11 (27.5)	18 (20.9)
Disease stage, *n* (%)		
c-stage III	9 (22.5)	18 (20.9)
c-stage IV	22 (55.0)	55 (64.0)
Postoperative recurrence	9 (22.5)	13 (15.1)
Driver mutation status, *n* (%)		
Wild type	33 (82.5)	73 (84.9)
EGFR (19 del or L858R)	7 (17.5)	12 (14.0)
ALK	0 (0)	1 (1.1)
Objective response at 9 weeks, *n* (%)		
CR or PR	11 (27.5)	12 (14.0)
SD	15 (37.5)	31 (36.0)
PD	14 (35.0)	43 (50.0)

Abbreviations: ALK, anaplastic lymphoma kinase; CR, complete response; c-stage, clinical stage; del, deletion.

cytocidal chemotherapy before nivolumab therapy, as per Japanese national insurance regulations from 2016 to 2018. After enrollment, 28 patients were excluded because no evaluable PBMC samples were available; 17 patients were excluded because the antitumor effect could not be assessed at 9 weeks after nivolumab therapy. Characteristics of all patients included in the discovery and validation cohorts are listed in **Table 1**.

To identify a biomarker that would distinguish patients presenting early disease progression after nivolumab treatment, we considered nonresponders the patients who showed disease progression and responders the patients who showed complete response (CR), PR, or SD according to CT evaluation at 9 weeks post nivolumab therapy. The patients presenting early disease progression by 9 weeks after therapy showed markedly poor survival, whereas SD and PR patients exhibited comparable and more favorable OS (Supplementary Fig. S2A and S2B). The nonresponders were a unique subgroup of patients who receive no survival benefit from nivolumab therapy.

We reported that CD4$^+$ T cells that downregulated CD62L expression (CD62L^{low}) in tumor-draining lymph nodes mediate potent antitumor reactivity when adoptively transferred in murine models and that the ratio of CD62L^{low} CD4$^+$ T cells to regulatory CD4$^+$ T cells in the peripheral blood correlates with disease stage and prognosis of SCLC (18–20). Consistent with our report, systemic T-cell immunity consisting of a CD62L^{low}CD44$^+$CD69$^+$CD90$^+$CD27^{low}T-bet$^+$CD4$^+$ T-cell subpopulation in tumors, tumor-draining lymph nodes, and the peripheral blood is required for antitumor immune responses (13). CD4$^+$ T cells of comparable phenotype were one of the three antitumor T-cell clusters in human melanoma-infiltrating lymphocytes (10). Thus, we examined this T-cell subset, specifically the CD62L^{low} subpopulations, in the peripheral blood of patients with NSCLC before nivolumab treatment.

Compared with nonresponders, nivolumab responders presented significantly higher CD62L^{low} cell percentages in the total populations of CD4$^+$ T cells (**Fig. 1B**, $P < 0.0001$) and CD8$^+$ T cells (**Fig. 1C**, $P = 0.0020$); conversely, the percentage of CD25$^+$FOXP3$^+$ cells in the total CD4$^+$ T-cell population was significantly higher ($P = 0.034$) in nonresponders (**Fig. 1D**). To develop a mathematical formula of nivolumab response prediction, we selected the percentage of CD62L^{low} cells in the total CD4$^+$ T-cell population as an independent factor because of the robust differences observed. The percentage of CD25$^+$FOXP3$^+$ cells in the total CD4$^+$ T-cell population was selected as another factor that constituted a T-cell cluster distinct from the CD62L^{low} CD4$^+$ T-cell cluster and negatively correlated with clinical outcome. We used the logistic regression model with the two selected factors to detect nonresponder patients and obtained the following formula: $[-31.3 + 12.0 \times \log$ [%CD62L^{low} T cells in total CD4$^+$ T-cell population: X] $- 6.1 \times \log$ [%CD25$^+$FOXP3$^+$ T cells in total CD4$^+$ T-cell population: Y]]; the formula approximately equaled $[-31.3 + 6.0 \times \log (X^2/Y)]$. Thus, we obtained the prediction formula with X^2/Y as the variable in the equation.

Formula values predict nivolumab responses

We determined the prediction formula values for responders and nonresponders (**Fig. 1E**, $P < 0.0047$) and performed ROC analysis for detecting nonresponders at 9 weeks within the discovery cohort (**Fig. 1F**). At the prediction formula threshold value of 192, which was obtained at the maximum likelihood ratio point of the ROC curve, sensitivity and specificity were 85.7% and 100%, respectively. We plotted the progression-free survival (PFS) and OS curves of patients identified as the responder type ($X^2/Y \geqq 192$) and nonresponder type ($X^2/Y < 192$) according to the analysis of PBMCs obtained before nivolumab treatment (**Fig. 1G** and **H**). Responders and nonresponders in the discovery cohort (threshold = 192) differed significantly ($P < 0.0001$) in terms of both PFS and OS. Next, we ascertained whether the prediction formula threshold value ($X^2/Y < 192$) could differentiate nonresponders in the independent validation cohort comprising 86 consecutive patients: the prediction formula values were significantly higher ($P = 0.0008$) in the case of responder than nonresponder patients in the validation cohort (**Fig. 1I**). In the validation cohort, responder-type patients showed significantly longer PFS (**Fig. 1J**, $P < 0.0001$) and OS (**Fig. 1K**, $P < 0.0001$) than nonresponder-type patients. All of the survival data ($n = 143$), including those for the patients who could not be evaluated for 9-week tumor responses, showed significant differences between nonresponder-type patients and responder-type patients (Supplementary Fig. S2C and S2D). ROC analysis of the prediction formula for detecting nonresponders at 9 weeks within the validation cohort ($n = 86$), and all of the evaluable patients were also performed ($n = 126$; Supplementary Fig. S2E and S2F). At the prediction formula threshold value of 192, sensitivity and specificity were 92.9% and 72.1% ($P < 0.0001$) in the validation formula, and 87.5% and 81.2% ($P < 0.0001$) in all of the evaluable patients. The objective responses and prediction formula results in relation to the histologic findings obtained for the patients ($n = 126$) are presented in Supplementary Table S2A. Multivariate analysis revealed that the prediction formula serves as an independent factor to correlate PFS and OS (Supplementary Table S2B).

CD62L^{low} CD4^{+} T-cell subset and other T-cell subpopulations

It was still unclear how CD62L could discriminate CD4^{+} T-cell subpopulations that predicted the antitumor responses of PD-1 blockade therapy. To define the CD62L^{low} CD4^{+} T-cell subsets and examine the relationship among the CD62L^{low} CD4^{+} T-cell subset and other T-cell subpopulations, we performed mass cytometry and microarray analysis in addition to FCM analysis. First, we analyzed the correlations among the percentages of T-cell subsets. Because CCR7 and CD45RA represent another standard for discriminating CCR7^{+}CD45RA^{+} naïve T cells, CCR7^{+}CD45RA^{-} central memory T cells (CM), CCR7^{-}CD45RA^{-} effector memory T cells (EM), and CCR7^{-} CD45RA^{+} effector T cells (EMRA), we examined their correlation with CD62L^{low} T-cell subsets. As described previously, CD8^{+} T cells were clearly divided into four subpopulations according to CD45RA and CCR7 expression, and the CD4^{+} T cells in the peripheral blood showed distinct patterns lacking the CD45RA^{+} CCR7^{-} subpopulation (ref. 16; **Fig. 2A** and **B**). The percentages of CD62L^{low} CD4^{+} T cells positively correlated ($P < 0.0001$) with the CCR7^{-} CD45RA^{-} EM subpopulation, but significantly negatively correlated with other CCR7^{+} CD45RA$^{-/+}$ subpopulations (**Fig. 2C** and **D**). The CCR7^{-}CD45RA^{-} CD4^{+} T-cell subgroup and CD62L^{low} CD4^{+} T-cell subgroup appear to comprise similar T-cell subsets; however, clinical outcome after nivolumab treatment showed no relationship with the percentages of CCR7^{-}CD45RA^{-} CD4^{+} T cells (Supplementary Fig. S3A and S3B). Next, we examined the correlation with Th1, Th2, and Th17 cells and Th follicular (Tfh) cells. The CD62L^{low} CD4^{+} T-cell subset significantly correlated with the CXCR3^{+}CCR4^{-}CCR6^{-} classical Th1 subset ($P < 0.0001$) but negatively correlated with the CXCR3^{-}CCR4^{+}CCR6^{-} Th2 subpopulation ($P = 0.0013$, **Fig. 2E–H**). The CD62L^{low} CD4^{+} T-cell subset also positively correlated with CD8^{+} T cells ($P < 0.0001$), the percentage of EMRA CD8^{+} T-cell subset ($P = 0.0091$), and CD62L^{low} CD8^{+} T-cell subset ($P < 0.0001$, **Fig. 2I–K**). The CCR7^{-}CD45RA^{-} CD4^{+} subpopulation weakly correlated with the Th1 subset ($P = 0.01$), but not Th2 population (Supplementary Fig. S3C and S3D). In line with these results, mass cytometry analysis revealed that the CD62L^{low}CD4^{+} cluster and CCR7^{-}CD4^{+} cluster were not identical (**Fig. 3A**). Unsupervised clustering analysis of gated CD4^{+}CD3^{+} T cells revealed that CD62L^{low}CD4^{+} T-cell subpopulation mostly belonged to CD27^{-}T-bet^{+}FOXP3^{-}CXCR3^{+}CCR4^{-}CCR6^{-} subpopulation. Contrarily, the

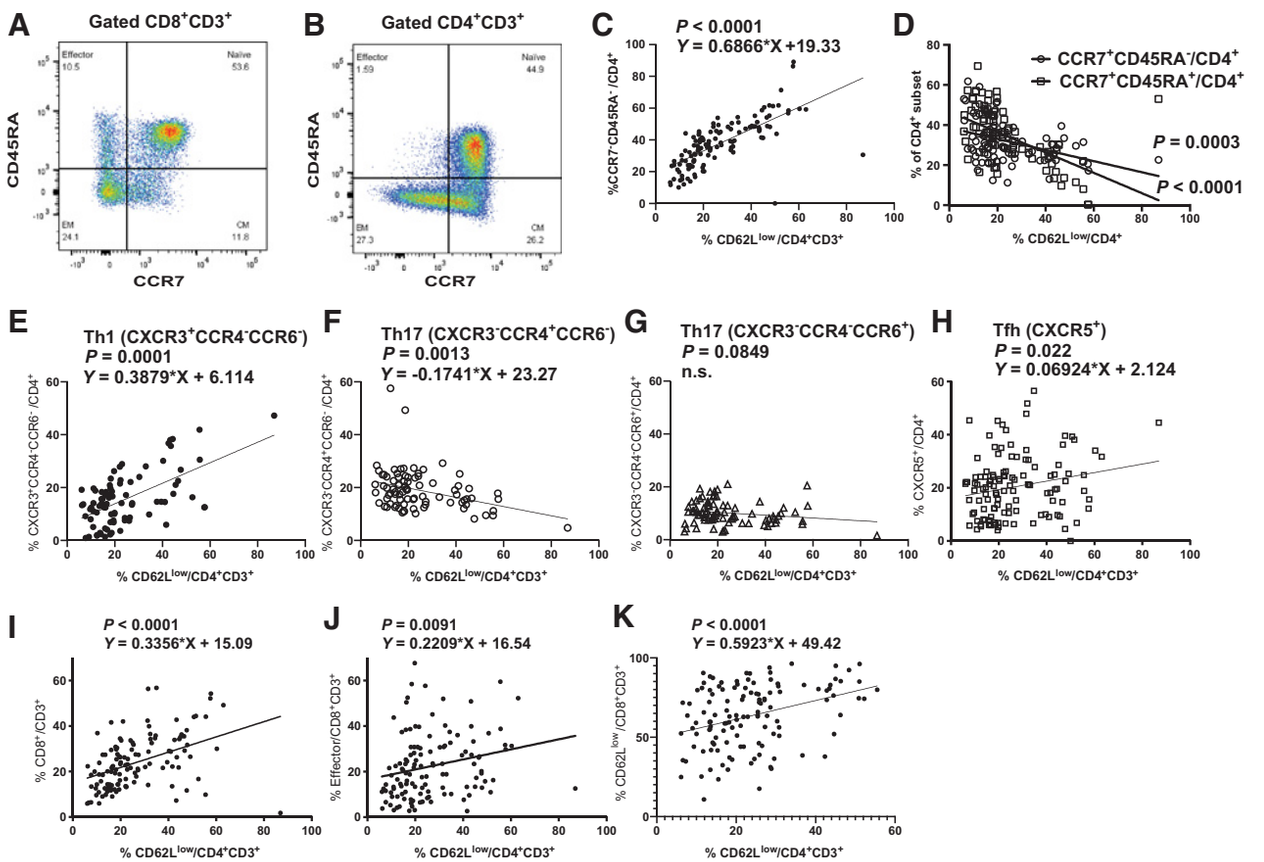

Figure 2.

Correlation between CD62L^{low} CD4^{+} T cells and other T-cell subpopulations. CCR7 and CD45RA expression on gated CD8^{+} CD3^{+} cells (**A**) and CD4^{+} CD3^{+} cells (**B**) among PBMCs. Linear correlations between the percentages of CD62L^{low}CD4^{+} cells and the percentages of CCR7^{-}CD45RA^{-} cells (**C**) and CCR7^{+}CD45RA^{-} or CCR7^{+}CD45RA^{+} cells (**D**) in the total population of CD4^{+} cells. Linear correlations between the percentages of CD62L^{low} CD4^{+} cells and the percentages of CXCR3^{+} CCR4^{-} CCR6^{-} cells (**E**), CXCR3^{-} CCR4^{+} CCR6^{-} cells (**F**), CXCR3^{-} CCR4^{-} CCR6^{+} cells (**G**), or CXCR5^{+} cells (**H**), respectively, in the total population of CD4^{+} cells. n.s., not signficant. Linear correlation between the percentages of CD62L^{low} CD4^{+} cells and the percentages of CD8^{+}CD3^{+} cells (**I**), (effector) CCR7^{-}CD45RA^{+} CD8^{+} cells (**J**), and CD62L^{low} CD8^{+} cells (**K**), respectively.

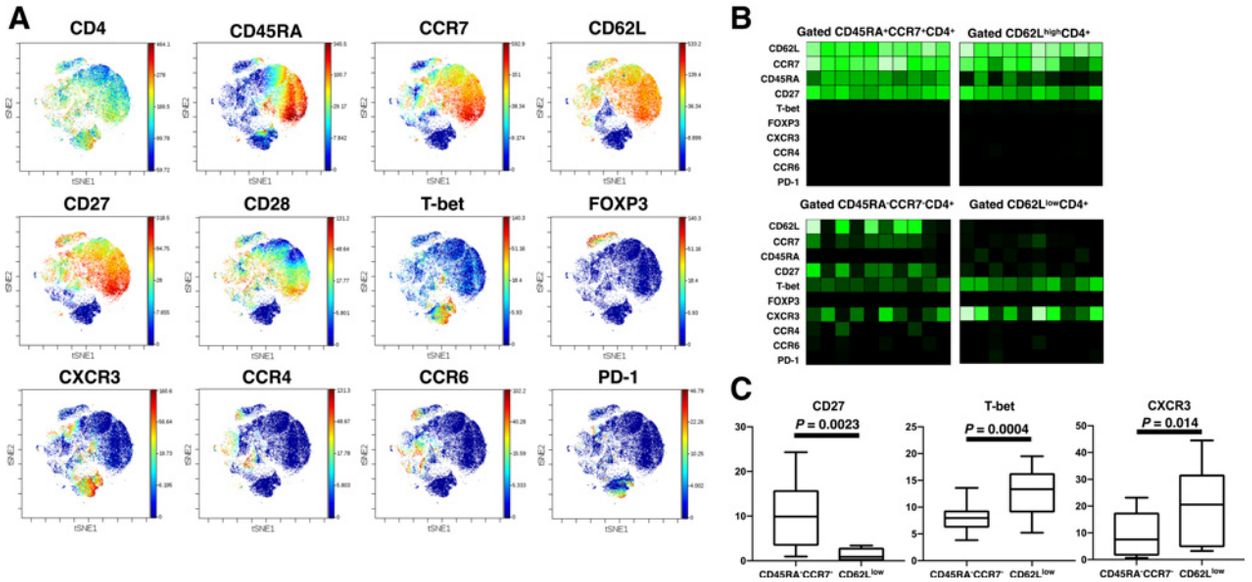

Figure 3.

Mass cytometry and gene expression analysis of CD4$^+$ T cells. **A,** Representative illustration of viSNE analysis for 10 patients for gated CD4$^+$CD3$^+$ cells upon unsupervised clustering according to the expression of 29 molecules (CD3, CD4, CD8, CD19, CD27, CD28, CD45RA, CD62L, CD69, CD80, CD90, CD103, CD134, CD137, CD152, CD154, CD183, CD194, CD196, CD197, CD223, CD273, CD274, CD278, CD279, T-bet, BCL-6, FOXP3, TIM-3). **B,** Heatmap demonstrating the average expression of CD62L, CCR7, CD45RA, CD27, T-bet, FOXP3, CXCR3, CCR4, CCR6, and PD-1 in gated CD45RA$^+$ CCR7$^+$, CD45RA$^-$ CCR7$^-$, CD62L^{high}, and CD62L^{low} CD4$^+$ CD3$^+$ T cells from 10 patients. **C,** Comparison of CD27, T-bet, and CXCR3 gene expression between gated CD45RA$^-$ CCR7$^-$ and CD62L^{low} CD4$^+$ CD3$^+$ T cells ($n = 10$). The box/whisker plots indicate median, upper quantile, and lower quantile. The lines indicate upper whiskers and lower whiskers.

CD45RA$^-$CCR7$^-$ subpopulation more broadly included CD27$^+$, T-bet$^-$, and FOXP3$^+$ subpopulations. Heatmap analysis to show the mean expression of molecules indicated that a significantly higher expression of T-bet and CXCR3 and significantly lower expression of CD27 was found in CD62L^{low}CD4$^+$ T cells compared with CD45RA$^-$CCR7$^-$CD4$^+$ T cells (**Fig. 3B** and **C**). It appears that a single marker of CD62L^{low}, but not CD45RA$^-$CCR7$^-$, could distinguish a relatively homogenous CD62L^{low}CD45RA$^-$ CCR7$^-$ CD27$^-$T-bet$^+$CXCR3$^+$CD4$^+$ T-cell subpopulation. We tested whether the CXCR3$^+$ CCR4$^-$ CCR6$^-$ Th1 subpopulation could predict responders, but there was no significant difference in the percentage of Th1 cells between responders and nonresponders (Supplementary Fig. S3E). It was likely that the CD62L^{low} subpopulation included both terminally differentiated Th1 and relatively immature, differentiating Th1 cells and that clinical responses required both of these.

As CD8$^+$ T cells play a critical role in eradicating cancer cells, we also examined the correlation between clinical responses and CD8$^+$ T-cell subsets. Unlike the CD4$^+$ T-cell subset, expression levels of CD62L and CCR7 on CD8$^+$ T cells were almost identical (Supplementary Fig. S3F). Thus, the CD62L^{low} CD8$^+$ T-cell subpopulation represents the EM+EMRA subpopulations. Whereas responders had significantly more CD62L^{low}CD8$^+$ T cells, this difference was not as robust as that for CD62L^{low}CD4$^+$ T cells (Supplementary Fig. S3G and S3H). CD62L^{low}CD4$^+$ T cells and CD62L^{low}CD8$^+$ T cells were significantly correlated (Supplementary Fig. S3I). Although the percentage of CD62L^{low}CD8$^+$ T cells correlated with PFS after nivolumab therapy, the correlation with CD62L^{low}CD4$^+$ T cells was more significant (Supplementary Fig. S3J and S3K).

Next, we examined the correlation of PD-1, LAG-3, and CTLA-4 expression with CD62L^{low}CD4$^+$ T cells. CD62L^{low} CD4$^+$ T cells, but not CCR7$^-$CD45RA$^-$CD4$^+$ T cells, positively correlated with PD-1 and LAG-3 expression on CD62L^{low}CD4$^+$ cells and PD-1 expression on CD8$^+$ T_{EMRA} cells (**Fig. 4A–C**; Supplementary Fig. S4A–S4C) and negatively correlated with CTLA-4 expression on CD62L^{low}CD4$^+$ T cells (**Fig. 4D**; Supplementary Fig. S4D).

CD62L^{low} CD4$^+$ T-cell gene expression in responder and nonresponder patients

Next, we performed microarray analysis to view CD62L^{low}CD4$^+$ T-cell differences at the molecular level between responder and nonresponder patients. We first elucidated gene expression differences in CD62L^{high}CD4$^+$ and CD62L^{low}CD4$^+$ T cells. CD62L^{high}CD4$^+$ T cells and CD62L^{low}CD4$^+$ T cells have distinct gene expression profiles (**Fig. 5A**). Consistent with previous reports, the majority of CD62L^{high}CD4$^+$ T cells were considered as naïve T cells because the C-C chemokine receptor type 7 (*CCR7*), *CD28*, and transcription factor 7 (*TCF7*) genes were highly expressed in CD62L^{high}CD4$^+$ T cells in all patients (**Fig. 5A**). CD62L^{low} CD4$^+$ T cells expressed more aurora kinase A (*AURKA*), C-C motif chemokine ligand 17 (*CCL17*), granzyme A, H (*GZMA, GZMH*), NADH dehydrogenase 2 (*ND2*), and *IL21* (**Fig. 5B**). Then, the genes in the signatures compared between the cells from PR and SD, PR and PD, SD and PD, PR + SD and PD, and PR and SD + PD (1,884, 1,826, 1,410, 1,167, and 1,513 genes, respectively) were merged into 3,458 genes (Supplementary Table S3). Among these, the expression of 30 of 53 of the genes that correlate with immune reactions, such as cytokines, cytokine receptors, chemokines, chemokine receptors, growth factors, costimulatory molecules, and immune checkpoint molecules, were significantly different in terms of nivolumab treatment response (**Fig. 5B**). These data indicated that C-type lectin domain family 2 member A (*CLEC2A*), *IL7*, IFNα (*IFNA*), C-X-C chemokine receptor type 3

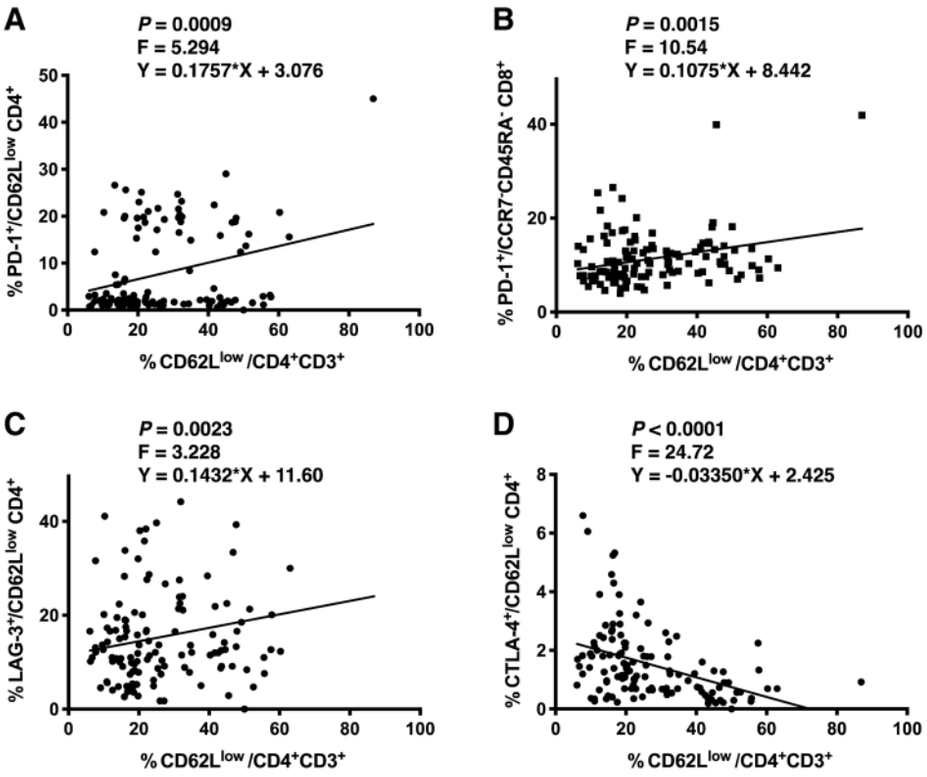

Figure 4.

Correlation between CD62L^{low} CD4^{+} T-cell subpopulation and PD-1, LAG3, and CTLA-4 expression and dendritic cell status. Correlations using simple linear regression analysis between the percentages of CD62L^{low} CD4^{+} cells and the percentages of indicated T-cell subpopulations (n = 84 for all). **A,** The percentage of CD62L^{low} in relation to the total number of CD4^{+}CD3^{+} cells as x-axis, and the percentages of PD-1^{+} cells in relation to the number of CD62L^{low}CD4^{+}CD3^{+} cells as y-axis. **B,** The percentages of PD-1^{+} cells in relation to the number of CCR7^{-} CD45RA^{-} CD8^{+}CD3^{+} cells. **C,** The percentages of LAG-3^{+} cells in relation to the number of CD62L^{low}CD4^{+}CD3^{+} cells. **D,** The percentages of CTLA-4^{+} cells in relation to number of CD62L^{low} CD4^{+} CD3^{+} cells.

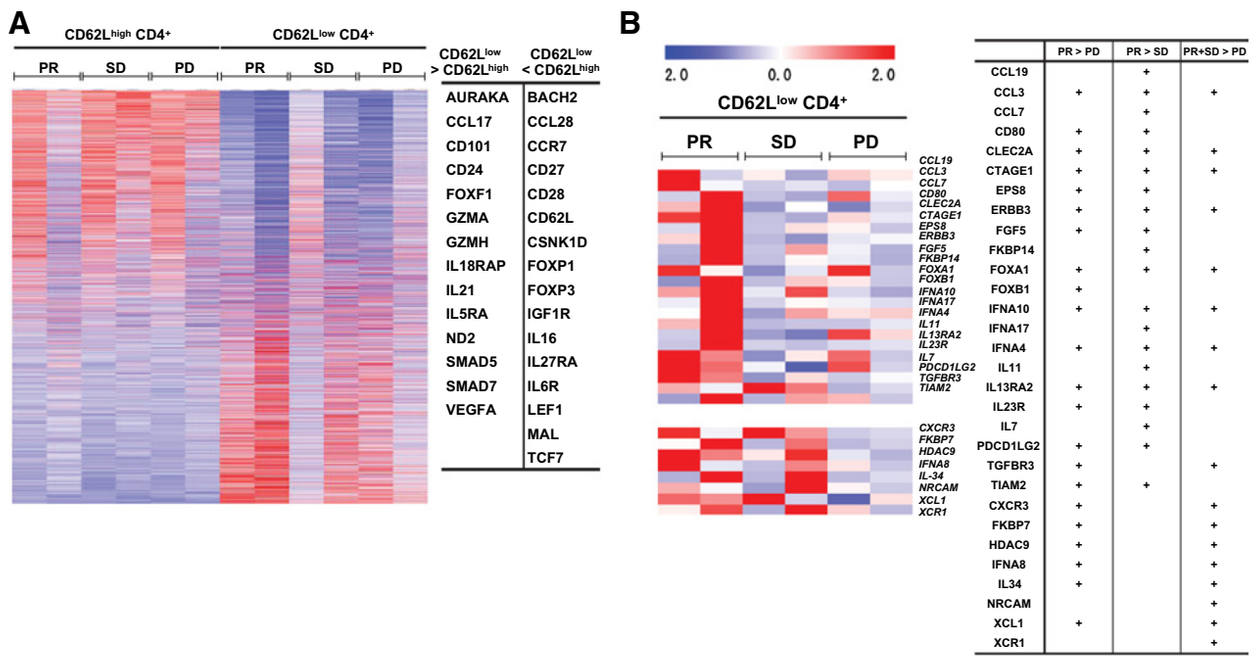

CD62L^{low} > CD62L^{high}	CD62L^{low} < CD62L^{high}
AURAKA	BACH2
CCL17	CCL28
CD101	CCR7
CD24	CD27
FOXF1	CD28
GZMA	CD62L
GZMH	CSNK1D
IL18RAP	FOXP1
IL21	FOXP3
IL5RA	IGF1R
ND2	IL16
SMAD5	IL27RA
SMAD7	IL6R
VEGFA	LEF1
	MAL
	TCF7

	PR > PD	PR > SD	PR+SD > PD
CCL19		+	
CCL3	+	+	+
CCL7		+	
CD80	+	+	
CLEC2A	+	+	+
CTAGE1	+	+	+
EPS8	+	+	
ERBB3	+	+	+
FGF5	+	+	
FKBP14		+	
FOXA1	+	+	+
FOXB1	+		
IFNA10	+	+	+
IFNA17		+	
IFNA4	+	+	+
IL11		+	
IL13RA2	+	+	+
IL23R	+	+	
IL7		+	
PDCD1LG2	+	+	
TGFBR3	+		+
TIAM2	+	+	
CXCR3	+		+
FKBP7	+		+
HDAC9	+		+
IFNA8	+		+
IL34	+		+
NRCAM			+
XCL1	+		+
XCR1			+

Figure 5.

Gene expressions correlated to response to nivolumab treatment. Gene signatures were obtained by comparing gene expression data between circulating CD62L^{high} CD4^{+} T cells and CD62L^{low} CD4^{+} T cells from PR, SD, and PD. **A,** Heatmap showing the expression of the genes expressed in CD62L^{low} CD4^{+} T cells and CD62L^{high} CD4^{+} T cells purified from the peripheral blood of the 6 patients consisting of 2 PR, 2 SD, and 2 PD patients. The genes that were expressed significantly higher in CD62L^{low} CD4^{+} T cells or CD62L^{high} CD4^{+} T cells are indicated. **B,** Heatmap showing the expression of the genes expressed in CD62L^{low} CD4^{+} T cells compared between PR to PD, PR to SD, and PR and SD to PD. + in the table indicates significant differences in gene expression between the groups.

(*CXCR3*), and histone deacetylase 9 (*HDAC9*) were preferentially expressed in CD62L^{low}CD4^{+} T cells derived from responders.

Long-term survivors and the CD62L^{low}CD4^{+} T-cell subpopulation

The nivolumab responding group contained both long-term survivors, whose PFS and OS curves featured a tail plateau, and short-term responders, who initially responded to nivolumab therapy but acquired resistance (**Fig. 1G** and **J**). Because CD4^{+} T cells were critical for predicting nonresponders of PD-1/PD-L1 blockade therapy, we examined CD4^{+} T cells obtained from patients after nivolumab therapy to investigate the differences between long-term survivors and short-term responders. Clinical trials with PD-1/PD-L1 blockade therapy have indicated that the tail plateau of PFS starts at 16–18 months after treatment (6, 7). Thus, we defined the patients who were progression-free for > 500 days as long-term responders and the patients who initially responded to treatment but acquired resistance and presented disease progression in the 500 days after nivolumab therapy as short-term responders. The long-term responders showed significantly higher numbers of pretreatment CD62L^{low}CD4^{+} T cells and prediction formula values compared with short-term responders (**Fig. 6A** and **B**). Next, to address the effect of PD-1 blockade therapy on T-cell subsets, we analyzed the peripheral blood obtained after nivolumab therapy. Surprisingly, at four weeks after nivolumab treatment, the percentage of the CD62L^{low}CD4^{+} T-cell subpopulation was significantly decreased in responder but not nonresponder patients

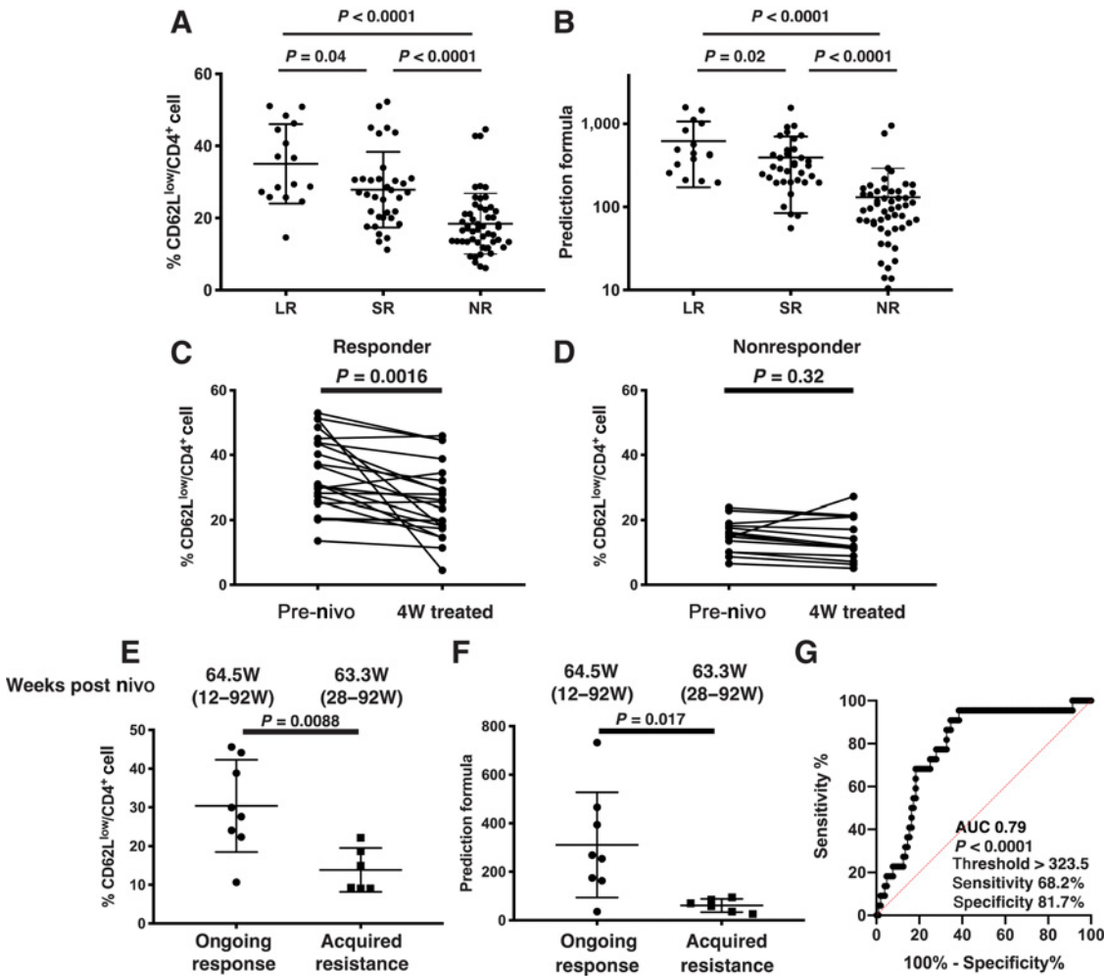

Figure 6.

CD62L^{low} CD4^{+} T-cell subpopulation in long-term survivors versus short-term responders. **A** and **B,** Percentages of CD62L^{low}CD4^{+} T cells and prediction formula values of pretreatment samples. Long-term responders (LR): patients who showed no disease progression for > 500 days ($n = 16$). Short-term responders (SR): patients who initially showed PR or SD for > 9 weeks but presented disease progression in the first 500 days after nivolumab treatment ($n = 34$). Nonresponders (NR): patients showing disease progression by 9 weeks after nivolumab therapy ($n = 52$). **C** and **D,** Comparison of the percentages of CD62L^{low} CD4^{+} T cells in PBMCs from responders and nonresponders obtained before and at 4 weeks after nivolumab treatment. **E** and **F,** Percentages of CD62L^{low} CD4^{+} T cells and prediction formula values of PBMC samples from 8 patients with ongoing responses to and 6 patients showing acquired resistance to nivolumab therapy. Data are presented as the means ± SEM. Symbols indicate values for individual patients. Statistical significance of differences was assessed using one-way ANOVA with Tukey *post hoc* analysis (**A** and **B**), using Student two-tailed paired *t* test (**C** and **D**), or using Student two-tailed unpaired *t* test (**E** and **F**). **G,** ROC curve of the formula that predicted long-term responders ($n = 126$). Sensitivity and specificity at the threshold value of the formula (323.5) were 68.2% and 81.7% ($P < 0.0001$), respectively. The red line indicates the line of identity.

(**Fig. 6C** and **D**). We examined PBMCs obtained from the 14 responder patients at 12–92 weeks after nivolumab therapy. At the time of PBMC collection, 6 patients showed disease progression and 8 patients still responded to the treatment. The ongoing responder patients maintained high percentages of $CD62L^{low}CD4^+$ T cells and prediction formula values (**Fig. 6E** and **F**). In contrast, the patients with acquired resistance showed decreased numbers of $CD62L^{low}$ $CD4^+$ T cells and prediction formula values (**Fig. 6E** and **F**). We performed ROC analysis to detect long-term responders (**Fig. 6G**). At the prediction formula threshold value of 323.5, which was obtained by determining the maximum likelihood ratio point of the ROC curve, sensitivity, and specificity were 68.2% and 81.7%, respectively. Thus, $CD4^+$ T-cell immunity evaluated with the peripheral blood samples before nivolumab therapy could predict RECIST responses and long-term survivors.

Discussion

Studies in cancer immunotherapy have focused on $CD8^+$ T cells in tumor microenvironment, because CTLs differentiate from $CD8^+$ T cells and induce tumor cell death upon tumor antigen recognition (12, 24, 25). However, in this study, we demonstrated that the $CD4^+$ T-cell immune status in the peripheral blood was a critical factor for determining the outcome of PD-1 blockade therapy in patients with NSCLC. In addition, the formula that accounted for the ratio between $CD62L^{low}$ and $CD25^+FOXP3^+$ $CD4^+$ T-cell percentages discriminated nivolumab nonresponders and long-term survivors. Accumulating evidence indicates that $CD4^+$ T cells are required for efficacious antitumor immunity, because $CD4^+$ T-cell help promotes priming, migratory potential, killing activity, and survival of CTLs (14, 26). To enhance the production, delivery, and killing activity of CTLs, it is likely that $CD4^+$ T cells are required systemically. mice that established antitumor immunity sufficient to eradicate tumors had $CD62L^{low}CD27^-T\text{-}bet^+CD44^+CD69^+CD90^+CD4^+$ T-cell clusters enriched through all the examined sites, mediating antitumor activity (13). Also, it was also demonstrated that continuous recruitment of antitumor T cells through peripheral blood is required for durable antitumor responses (13). In addition, melanoma-infiltrating lymphocytes with almost the same phenotype of $CD4^+$ T cells, $CD62L^{low}CD27^-$ $FOXP3^-$ $CD44^+$ $CXCR3^+$ $ICOS^+$ $T\text{-}bet^+$, correlated with responses to immune checkpoint inhibitors (10). In line with these studies, our mass cytometry study showed that the majority of $CD62L^{low}$ $CD4^+$ T cells were $T\text{-}bet^+$, $CD27^-$, $FOXP3^-$, and $CXCR3^+$ in the $CD4^+$ population. In contrast, the $CCR7^-$ $CD4^+$ T-cell subpopulation, which did not show differences between nonresponders and responders, included more broad subpopulations, such as $T\text{-}bet^-$, $CD27^+$, and $FOXP3^+$ subpopulations. The $CD62L^{low}$ $CD4^+$ T-cell subpopulation significantly correlated with $CXCR3^+CCR4^-CCR6^-$ cells, thus, the $CD62L^{low}$ $CD4^+$ T-cell subpopulation likely plays a critical role in cellular immunity as Th1 cells. Accordingly, the $CD62L^{low}$ $CD4^+$ T-cell subpopulation positively correlated with the percentages of effector $CD8^+$ T cells. The $CD62L^{low}$ $CD4^+$ T-cell subpopulation positively correlated with the expression of PD-1, but negatively with that of CTLA-4. Thus, the $CD62L^{low}CD27^-FOXP3^-CXCR3^+$ $T\text{-}bet^+$ $CD4^+$ T-cell subset likely comprised Th1 cells and effector $CD8^+$ T cells, indicating that they were regulated by PD-1 but not CTLA-4.

A limitation of this study is that the antigenic specificity of $CD62L^{low}$ T cells was not tested owing to the small size of the tumor specimens obtained. We previously reported that $CD62L^{low}$, but not $CD62L^{high}$ T cells, secreted IFNγ in a tumor antigen–specific manner, mediating therapeutic efficacy when infused intravenously into murine models (18, 19). T cells were derived from the peripheral blood of patients with small-cell lung cancer and it was found that $CD62L^{low}$ T cells, but not $CD62L^{high}$ T cells, secreted IFNγ in the presence of autologous tumor cells (20).

It was unexpected that the percentages of $CD62L^{low}CD4^+$ T cells decreased in responder but not nonresponder patients after nivolumab therapy, because $PD\text{-}1^+$ effector $CD8^+$ T cells increase after effective anti-PD-1 therapy in the peripheral blood (27). However, PD-1 blockade therapy increased only the $CD8^+$ antitumor T-cell clusters, not the $CD4^+$ antitumor T-cell clusters in melanoma-infiltrating lymphocytes; therefore, it is possible that PD-1 blockade therapy is not capable of facilitating antitumor $CD4^+$ T-cell proliferation. Tumor mutational burden decreases in responder patients after nivolumab therapy; effective PD-1 blockade therapy seems to invigorate the immune-editing process, resulting in the loss of cancer clones featuring high mutation burdens (28). Thus, it is likely that our findings indicated the consequent loss of the specific effector T cells due to the loss of cancer-associated antigens. Because only the patients who retained $CD62L^{low}$ $CD4^+$ T cells exhibited an ongoing antitumor response during nivolumab therapy, one of the mechanisms underlying acquired resistance might involve the loss of tumor-associated antigens resulting in the depletion of $CD4^+$ T-cell help. Our study revealed that the patients who presented high percentages of $CD62L^{low}$ $CD4^+$ T cells before nivolumab therapy and maintained the $CD62L^{low}$ $CD4^+$ T-cell subpopulation tended to survive for >500 days without disease progression. A promising therapy could thus entail increasing the $CD62L^{low}CD4^+$ T-cell subpopulation with treatment, for example, anti-CTLA-4 therapy, while concurrently monitoring the peripheral blood T-cell subpopulation.

Gene expression analysis revealed that gene expression profiles differed between $CD62L^{high}$ and $CD62L^{low}$ $CD4^+$ T cells. $CD62L^{low}$ $CD4^+$ T cells expressed the gene encoding *AURORKA, CD101, GZMA*, and *GZMH, ND2*, and *IL21*. *AURORKA* is expressed in mitotic cells during G_2–M phase and is required for maintaining Lck active after TCR engagement in T cells (29). Granzyme A and H are expressed in cells that have killing activity, such as CTLs. Activated $CD4^+$ T cells can express granzyme and mediate antitumor reactivity (30). ND2 is one of seven mitochondrially encoded subunits of the enzyme NADH dehydrogenase (31). IL21 is demonstrated to enhance and sustain $CD8^+$ T-cell response resulting in durable antitumor immunity (32). Taken together, the $CD62L^{low}$ $CD4^+$ T-cell subset included proliferating T cells after activation through TCR engagement, which exhibited effector functions and enhanced $CD8^+$ T-cell killing activity. Some genes, such as *CCL19, IL7, CXCR3, CLEC2A, TGFBR3*, and *HDAC9,* were preferentially expressed in PR and/or SD-derived $CD62L^{low}CD4^+$ T cells. CCL19 binds to CCR7 and attracts certain cell of the immune system, including dendritic cells, and $CCR7^+$ central memory cells (33, 34). Signaling of IL7, a nonredundant cytokine for T-cell proliferation, promotes antitumor T-cell immunity (35, 36). Interestingly, IL7 and CCL19 expression in CAR-T cells improves immune cell infiltration and CAR-T survival in the tumor (37). CLEC2A enhances TCR-stimulated T-cell expansion by increasing their survival (38). TGFβ has widespread regulatory activity affecting multiple types of immune cells with soluble TGFBR3 potentially inhibiting TGFβ signaling (39). HDAC9 controls FOXP3 expression and suppresses Treg function (40). These molecules thus appear to play a role in facilitating T-cell activation, inhibiting regulatory mechanisms, and increasing the quantity of antitumor effector T cells, potentially representing promising targets to enhance antitumor immunotherapy.

In conclusion, we have demonstrated that the systemic CD4$^+$ T-cell immunity monitoring with the peripheral blood predicted anti-PD-1 therapy responses in patients with NSCLC. We have developed a formula based on CD62L^{low} CD4$^+$ T-cell and Treg percentages that could serve as a biomarker for predicting treatment outcome in these patients. Our findings hold clinical implications, as they support anti-PD-1 therapy for patients with NSCLC with high numbers of circulating CD62L^{low} CD4$^+$ T cells and provide the foundation for new treatment strategies for patients presenting distinct CD4$^+$ T-cell immune statuses.

Disclosure of Potential Conflicts of Interest

S. Kitano reports receiving commercial research grants from Eisai, Boehringer Ingelheim, Astellas Pharma, Gilead Sciences, Regeneron, Takara Bio, Ono Pharmaceutical, and Daiichi Sankyo, speakers bureau honoraria from Nippon Kayaku, Boehringer Ingelheim, Meiji Seika Pharma, Taiho, Novartis, Daiichi Sankyo, MSD, Kyowa Hakko Kirin, Celgene, Eisai, Ono Pharmaceutical, Bristol-Myers Squibb, Regeneron, AYUMI Pharmaceutical Corporation, Rakuten Medical, GlaxoSmithKline, AstraZeneca, Chugai, Pfizer, Sanofi, and Sumitomo Dainippon Pharma, and other remuneration from Pharmaceuticals and Medical Devices Agency (PMDA). O. Yamaguchi reports receiving speakers bureau honoraria from Ono Pharmaceutical, Bristol-Myers Squibb, Taiho Pharmaceutical, MSD, Chugai Pharmaceutical, and AstraZeneca. K. Kobayashi reports receiving speakers bureau honoraria from AstraZeneca, Boehringer Ingelheim, Bristol-Myers Squibb, Taiho Pharmaceutical, and Ono Pharmaceutical. No potential conflicts of interest were disclosed by the other authors.

Authors' Contributions

Conception and design: O. Yamaguchi, K. Yoshimura
Development of methodology: S. Kitano, K. Fukui
Acquisition of data (provided animals, acquired and managed patients, provided facilities, etc.): O. Yamaguchi, A. Shiono, A. Mouri, F. Nishihara, Y. Miura, K. Hashimoto, Y. Murayama, K. Kobayashi
Analysis and interpretation of data (e.g., statistical analysis, biostatistics, computational analysis): H. Kagamu, S. Kitano, K. Yoshimura, K. Horimoto, M. Kitazawa, K. Kaira
Writing, review, and/or revision of the manuscript: H. Kagamu, S. Kitano, K. Yoshimura, K. Horimoto, K. Kaira
Administrative, technical, or material support (i.e., reporting or organizing data, constructing databases): K. Yoshimura
Study supervision: S. Kitano

Acknowledgments

This work was supported in part by JSPS KAKENHI grant number 17H04184. In addition, this work was supported in part by the Japan Agency for Medical Research and Development (grant nos. 18ae0101016s0105 and 19ae0101074h0001). We thank Mrs. Koko Kodaira for technical assistance.

The costs of publication of this article were defrayed in part by the payment of page charges. This article must therefore be hereby marked *advertisement* in accordance with 18 U.S.C. Section 1734 solely to indicate this fact.

Received July 27, 2019; revised September 18, 2019; accepted December 17, 2019; published first December 23, 2019.

References

1. Wolchok JD, Kluger H, Callahan MK, Postow MA, Rizvi NA, Lesokhin AM, et al. Nivolumab plus ipilimumab in advanced melanoma. N Engl J Med 2013;369:122–33.
2. Robert C, Long GV, Brady B, Dutriaux C, Maio M, Mortier L, et al. Nivolumab in previously untreated melanoma without BRAF mutation. N Engl J Med 2015;372:320–30.
3. Ferris RL, Blumenschein G Jr, Fayette J, Guigay J, Colevas AD, Licitra L, et al. Nivolumab for recurrent squamous-cell carcinoma of the head and neck. N Engl J Med 2016;375:1856–67.
4. Motzer RJ, Escudier B, McDermott DF, George S, Hammers HJ, Srinivas S, et al. Nivolumab versus everolimus in advanced renal-cell carcinoma. N Engl J Med 2015;373:1803–13.
5. Kang YK, Boku N, Satoh T, Ryu MH, Chao Y, Kato K, et al. Nivolumab in patients with advanced gastric or gastro-oesophageal junction cancer refractory to, or intolerant of, at least two previous chemotherapy regimens (ONO-4538-12, ATTRACTION-2): a randomised, double-blind, placebo-controlled, phase 3 trial. Lancet 2017;390:2461–71.
6. Brahmer J, Reckamp KL, Baas P, Crino L, Eberhardt WE, Poddubskaya E, et al. Nivolumab versus docetaxel in advanced squamous-cell non-small-cell lung cancer. N Engl J Med 2015;373:123–35.
7. Borghaei H, Paz-Ares L, Horn L, Spigel DR, Steins M, Ready NE, et al. Nivolumab versus docetaxel in advanced nonsquamous non-small-cell lung cancer. N Engl J Med 2015;373:1627–39.
8. Rittmeyer A, Barlesi F, Waterkamp D, Park K, Ciardiello F, von Pawel J, et al. Atezolizumab versus docetaxel in patients with previously treated non-small-cell lung cancer (OAK): a phase 3, open-label, multicentre randomised controlled trial. Lancet 2017;389:255–65.
9. Reck M, Rodriguez-Abreu D, Robinson AG, Hui R, Csoszi T, Fulop A, et al. Pembrolizumab versus chemotherapy for PD-L1-positive non-small-cell lung cancer. N Engl J Med 2016;375:1823–33.
10. Wei SC, Levine JH, Cogdill AP, Zhao Y, Anang NAS, Andrews MC, et al. Distinct cellular mechanisms underlie anti-CTLA-4 and anti-PD-1 checkpoint blockade. Cell 2017;170:1120–33.
11. Wu SP, Liao RQ, Tu HY, Wang WJ, Dong ZY, Huang SM, et al. Stromal PD-L1-positive regulatory T cells and PD-1-positive CD8-positive T cells define the response of different subsets of non-small cell lung cancer to PD-1/PD-L1 blockade immunotherapy. J Thorac Oncol 2018;13:521–32.
12. Thommen DS, Koelzer VH, Herzig P, Roller A, Trefny M, Dimeloe S, et al. A transcriptionally and functionally distinct PD-1(+) CD8(+) T cell pool with predictive potential in non-small-cell lung cancer treated with PD-1 blockade. Nat Med 2018;24:994–1004.
13. Spitzer MH, Carmi Y, Reticker-Flynn NE, Kwek SS, Madhireddy D, Martins MM, et al. Systemic immunity is required for effective cancer immunotherapy. Cell 2017;168:487–502.
14. Borst J, Ahrends T, Babala N, Melief CJM, Kastenmuller W. CD4(+) T cell help in cancer immunology and immunotherapy. Nat Rev Immunol 2018;18:635–47.
15. Chen DS, Mellman I. Oncology meets immunology: the cancer-immunity cycle. Immunity 2013;39:1–10.
16. Sallusto F, Lenig D, Forster R, Lipp M, Lanzavecchia A. Two subsets of memory T lymphocytes with distinct homing potentials and effector functions. Nature 1999;401:708–12.
17. Bradley LM, Watson SR, Swain SL. Entry of naive CD4 T cells into peripheral lymph nodes requires L-selectin. J Exp Med 1994;180:2401–6.
18. Kagamu H, Touhalisky JE, Plautz GE, Krauss JC, Shu S. Isolation based on L-selectin expression of immune effector T cells derived from tumor-draining lymph nodes. Cancer Res 1996;56:4338–42.
19. Kagamu H, Shu S. Purification of L-selectin(low) cells promotes the generation of highly potent CD4 antitumor effector T lymphocytes. J Immunol 1998;160:3444–52.
20. Koyama K, Kagamu H, Miura S, Hiura T, Miyabayashi T, Itoh R, et al. Reciprocal CD4$^+$ T-cell balance of effector CD62L^{low} CD4$^+$ and CD62L^{high}CD25$^+$ CD4$^+$ regulatory T cells in small cell lung cancer reflects disease stage. Clin Cancer Res 2008;14:6770–9.
21. Kamada T, Togashi Y, Tay C, Ha D, Sasaki A, Nakamura Y, et al. PD-1(+) regulatory T cells amplified by PD-1 blockade promote hyperprogression of cancer. Proc Natl Acad Sci U S A 2019;116:9999–10008.
22. Aggarwal CC. Outlier analysis. New York: Springer; 2017. p. 466.
23. Daszykowski M, Kaczmarek K, Vander Heyden Y, Walczak B. Robust statistics in data analysis — a review. Chemometr Intell Lab Syst 2007;85:203–19.
24. Ahmadzadeh M, Johnson LA, Heemskerk B, Wunderlich JR, Dudley ME, White DE, et al. Tumor antigen-specific CD8 T cells infiltrating the tumor express high levels of PD-1 and are functionally impaired. Blood 2009;114:1537–44.
25. Gros A, Robbins PF, Yao X, Li YF, Turcotte S, Tran E, et al. PD-1 identifies the patient-specific CD8(+) tumor-reactive repertoire infiltrating human tumors. J Clin Invest 2014;124:2246–59.
26. Takeuchi Y, Tanemura A, Tada Y, Katayama I, Kumanogoh A, Nishikawa H. Clinical response to PD-1 blockade correlates with a sub-fraction of peripheral

central memory CD4+ T cells in patients with malignant melanoma. Int Immunol 2018;30:13–22.
27. Kamphorst AO, Pillai RN, Yang S, Nasti TH, Akondy RS, Wieland A, et al. Proliferation of PD-1+ CD8 T cells in peripheral blood after PD-1-targeted therapy in lung cancer patients. Proc Natl Acad Sci U S A 2017;114:4993–8.
28. Riaz N, Havel JJ, Makarov V, Desrichard A, Urba WJ, Sims JS, et al. Tumor and microenvironment evolution during immunotherapy with nivolumab. Cell 2017;171:934–49.
29. Blas-Rus N, Bustos-Moran E, Perez de Castro I, de Carcer G, Borroto A, Camafeita E, et al. Aurora A drives early signalling and vesicle dynamics during T-cell activation. Nat Commun 2016;7:11389.
30. Hirschhorn-Cymerman D, Budhu S, Kitano S, Liu C, Zhao F, Zhong H, et al. Induction of tumoricidal function in CD4+ T cells is associated with concomitant memory and terminally differentiated phenotype. J Exp Med 2012;209: 2113–26.
31. Chomyn A, Cleeter MW, Ragan CI, Riley M, Doolittle RF, Attardi G. URF6, last unidentified reading frame of human mtDNA, codes for an NADH dehydrogenase subunit. Science 1986;234:614–8.
32. Moroz A, Eppolito C, Li Q, Tao J, Clegg CH, Shrikant PA. IL-21 enhances and sustains CD8+ T cell responses to achieve durable tumor immunity: comparative evaluation of IL-2, IL-15, and IL-21. J Immunol 2004;173:900–9.
33. Luther SA, Bidgol A, Hargreaves DC, Schmidt A, Xu Y, Paniyadi J, et al. Differing activities of homeostatic chemokines CCL19, CCL21, and CXCL12 in lymphocyte and dendritic cell recruitment and lymphoid neogenesis. J Immunol 2002; 169:424–33.
34. Haessler U, Pisano M, Wu M, Swartz MA. Dendritic cell chemotaxis in 3D under defined chemokine gradients reveals differential response to ligands CCL21 and CCL19. Proc Natl Acad Sci U S A 2011;108:5614–9.
35. von Freeden-Jeffry U, Vieira P, Lucian LA, McNeil T, Burdach SE, Murray R. Lymphopenia in interleukin (IL)-7 gene-deleted mice identifies IL-7 as a nonredundant cytokine. J Exp Med 1995;181:1519–26.
36. Shum T, Omer B, Tashiro H, Kruse RL, Wagner DL, Parikh K, et al. Constitutive signaling from an engineered IL-7 receptor promotes durable tumor elimination by tumor redirected T-cells. Cancer Discov 2017;7:1238–47.
37. Adachi K, Kano Y, Nagai T, Okuyama N, Sakoda Y, Tamada K. IL-7 and CCL19 expression in CAR-T cells improves immune cell infiltration and CAR-T cell survival in the tumor. Nat Biotechnol 2018;36:346–51.
38. Huarte E, Cubillos-Ruiz JR, Nesbeth YC, Scarlett UK, Martinez DG, Engle XA, et al. PILAR is a novel modulator of human T-cell expansion. Blood 2008;112: 1259–68.
39. Lopez-Casillas F, Cheifetz S, Doody J, Andres JL, Lane WS, Massague J. Structure and expression of the membrane proteoglycan betaglycan, a component of the TGF-beta receptor system. Cell 1991;67:785–95.
40. Beier UH, Akimova T, Liu Y, Wang L, Hancock WW. Histone/protein deacetylases control Foxp3 expression and the heat shock response of T-regulatory cells. Curr Opin Immunol 2011;23:670–8.